JOURNAL OF AIRCRAFT
Vol. 44, No. 5, September–October 2007

Engineering Notes

ENGINEERING NOTES are short manuscripts describing new developments or important results of a preliminary nature. These Notes should not exceed 2500 words (where a figure or table counts as 200 words). Following informal review by the Editors, they may be published within a few months of the date of receipt. Style requirements are the same as for regular contributions (see inside back cover).

Passive Control of Bluff Body Using Stepped-Nose Obstacle

A. Rehman* and K. Kontis†
University of Manchester, Manchester, M60 1QD England, United Kingdom

DOI: 10.2514/1.30332

Introduction

A REGION of separated flow occurs over a large part of the surface of a bluff body, which results in a large wake. The size of this wake has a proportional influence on the amount of pressure drag. Several control methodologies have been suggested in the past to modify the flow over a bluff body to achieve drag reduction, either with passive geometrical modifications or with active techniques [1–3]. The objectives of the present study are to 1) validate the experimental predictions of [3] using numerical simulations, and 2) examine the control effectiveness of the stepped-nose obstacle on the vortex shedding process.

Computational Approach

Flow was assumed to be incompressible, viscous, two-dimensional, and unsteady. There is no external source that transfers heat into the system, therefore the energy equation was not considered. The segregated solver in Fluent 6.2 was selected [4]. The implicit method was used. By using this method, all the fluxes and source terms were evaluated in terms of the unknown variable values at the new time level. The pressure and velocity were coupled using the Simple algorithm. For the discretization of the model equations, the Quick scheme was used instead of the first-order or second-order upwind scheme [5,6]. The time step was set to 0.0001 s. Gambit was used to create the geometric model as described in [3], see also Fig. 1. All lengths were made dimensionless with the length L of the rectangular bluff body. The model was placed at the center of the computational domain. Each lateral boundary was located at $10L$ from the center of the domain. The inflow and outflow boundaries were located $10L$ upstream and $20L$ downstream of the model, respectively. The effects of a smaller domain size with an upstream length of $5L$, a downstream length of $4L$, and a width of $7L$ were also accessed. Both domains exhibited similar flow patterns and the computed time-averaged results deviated only 1% [6]. The present analysis used the larger domain.

Two nondimensional step lengths of $\ell/L = 0.08$ (small step configuration, SSC) and $\ell/L = 0.24$ (large step configuration, LSC) were employed to demonstrate their effectiveness over the baseline configuration (BC). The nondimensional step height $h/L = 0.16$ was kept constant. Velocity inlet and outflow boundary conditions were used at the inlet and exit, respectively. A symmetry boundary condition was defined for the upper and lower boundaries, whereas the surface of the model was modeled as a wall. For all simulations, the flowfield was initialized from the inlet boundary conditions. Because only the drag coefficient C_D was available from [3] for the BC case, the computed time-averaged C_D was used to determine the most suitable turbulence model. Table 1 shows the comparison of the results for the BC case. The k–ω model was selected for the present study. To evaluate the grid sensitivity of the solution, initially three grids were analyzed. Table 2 shows the grid independence analysis. In all cases, a grid spacing adjacent to the surface corresponded to $Y^+ = 1.0$ was achieved. The grid with 80,000 nodes was selected as the difference on the computed time-averaged C_D with the 120,000 nodes grid was less than 1%. The freestream velocity was 10 m/s. The Reynolds number was 5.0×10^4 based on the bluff body length L and freestream flow velocity.

Results and Discussion

Figures 2 and 3 show the numerical flow visualization results for the three cases considered (where X/L and Y/L are the nondimensional Cartesian coordinates). In the BC case, the flow separates at the leading-edge corners and separation bubbles are present within the shear layers. As a result, a large wake is formed (Fig. 2a). The vorticity contours revealed an unsteady periodic flow structure in which the separated vortices are shed alternately from the upper and lower sides (Fig. 2b). In the SSC case, the separated flow at the leading corners reattaches to either side of the main body just close to the trailing-edge corners indicating a reduced wake width compared with the BC case [6]. The separated vortices are shed alternately from the upper and lower sides indicating a very small change in flow pattern compared with the BC case [6]. Therefore, a significant recirculation region exists at either lateral side of the body, and the wake size is still significantly large. On the other hand, a significant difference in the flow patterns was observed for the LSC case (Fig. 3). The flow smoothly reattaches to the lateral sides of the body, as shown in Fig. 3a, leading to an effective reduction in the wake width as compared with the BC case. As a result of the reduced wake width, the vortex shedding process was confined to a very narrow path as compared with the BC and SSC cases (Fig. 3b). Therefore, from the qualitative observations, it is obvious that the stepped-nose obstacle suppresses the large-scale flow separation on both sides of the body.

The time-averaged computed surface pressure coefficient C_P distribution is shown in Fig. 4. At the center of the body's back surface, the pressure coefficient increased from -1.5 (BC case) to -1.3 (SSC case) and -0.84 (LSC case). The suction pressure acting at the back surface decreased with increasing step length. This suggests reattachment of flow, which leads to pressure recovery along either side of the body. The time-averaged streamwise velocity distributions indicated the existence of a thin and stable boundary layer on the sides of the body for the LSC case; whereas for the SSC

Received 7 February 2007; revision received 3 May 2007; accepted for publication 12 May 2007.

*Research Student, Aerophysics and Advanced Measurement Technology Laboratory, School of Mechanical, Aerospace, and Civil Engineering, Post Office Box 88.

†Senior Lecturer, Associate Professor, Head of the Aerophysics and Advanced Measurement Technology Laboratory and Advanced Flow Diagnostics Research Group. Member AIAA.

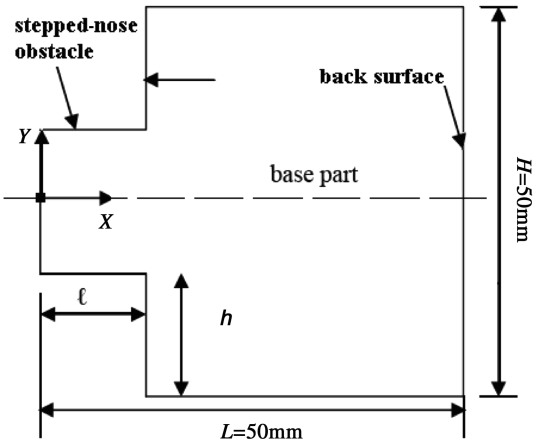

Fig. 1 Model geometry with stepped-nose obstacle.

case, it indicated that the flow separates again after its reattachment on the side surfaces immediately downstream of the leading-edge corners, forming a large-scale circulation region along each side surface [6]. For the BC case, the time-averaged streamwise velocity distributions indicated the existence of a thick and unstable boundary layer along the side surfaces of the model. The turbulence intensity near the side surfaces for the LSC case has approximately the same value (2%) as that in the freestream. The Reynolds stress levels are small, indicating the existence of attached flow on the lateral sides. However, the higher turbulence intensity and Reynolds stress levels near the lateral sides for the SSC and BC indicated the existence of a large-scale flow separation region [6], which supports the findings of the numerical flow visualization.

Based on the computed quantities and numerical flow visualization just presented, it is evident that the reattachment of the flow in the lateral sides causes reduction of the turbulent wake and the subsequent reduction in drag as shown in Fig. 5. Figure 5 also indicates that the time-averaged computed drag coefficient decreases with increasing step length. The computed time-averaged net drag coefficient for the LSC and SSC cases is 0.8 and 2, respectively, indicating a reduction of drag of more than 66 and 10% for LSC and SSC cases, respectively, compared with the BC case. Thus the computed results suggest that the stepped-nose obstacle of $\ell/L = 0.24$ and $h/L = 0.16$ can significantly reduce the drag coefficient compared with that of the BC case. The results are compared with the experiment in [3] and are consistent with the qualitative observations presented in Figs. 2 and 3.

The percentage error with respect to the experimental results has been computed to assess the fidelity of the k–ω SST model in predicting the quantities previously discussed and presented in Figs. 2–5. The error was found to be in the region of 6–8%, and 3–5.5% for the SSC and LSC cases, respectively, indicating that the k–ω SST predicted the flow quantitatively and the computed results are in good agreement with experiment. The high-percentage error in the time-averaged computed C_D can be explained by the fact that

Table 1 Comparisons of drag coefficient for the BC case

Turbulence model	Computed C_D	C_D, exp. [3]
k–ω SST	2.38	2.2
k–ε Renormalization group	2.45	

Table 2 Grid independence analysis

Turbulence model	Grid, no. of nodes	Computed C_D	C_D, exp. [3]
k–ω SST	60,000	2.47	2.2
	80,000	2.38	
	120,000	2.36	

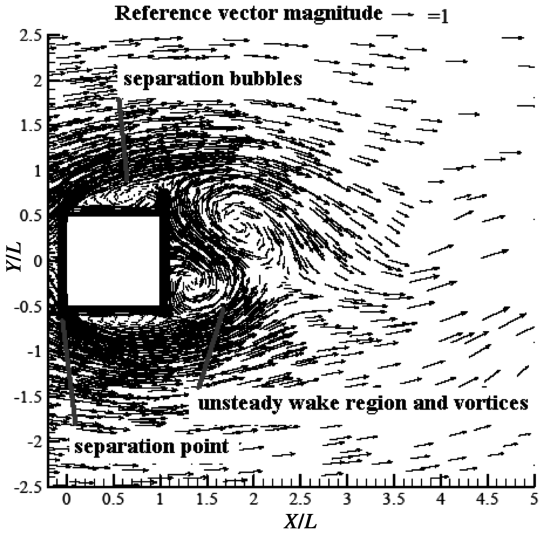

a) Computed velocity field

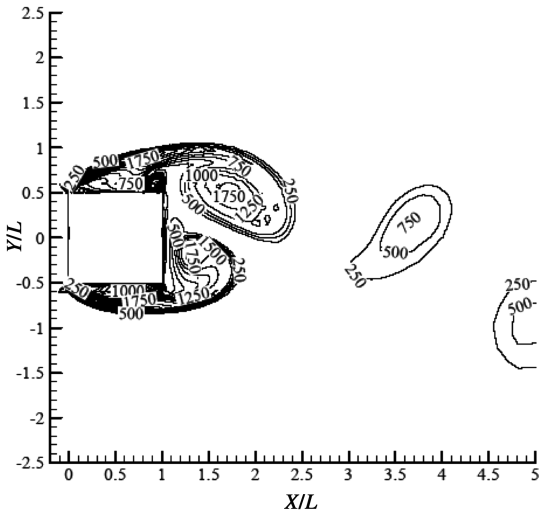

b) Vorticity contours

Fig. 2 Numerical flow visualization results for BC case.

beyond a certain value of Reynolds number, the wake of two-dimensional bodies becomes susceptible to a primary three-dimensional Floquet-type instability mechanism, which leads to the amplification of three-dimensional disturbances and eventual development of strong streamwise-oriented vortical structures [6–8]. Thus, two-dimensional simulations which do not allow the existence of these streamwise vortices fail to accurately predict even gross quantities such as mean drag [9]. However, the numerical visualization study, presented in Figs. 2 and 3, revealed that Fluent 6.2 together with the k–ω SST model can predict the flow events such as separation, reattachment, and the vortex shedding process very well.

Conclusions

The study indicated that the stepped-nose obstacle can prevent large-scale flow separation on the lateral sides of a bluff body and reduce drag more than 66%. The optimum step length and height combination plays an important role in the control effectiveness of this device. For the LSC case, the vortex shedding process was confined to a very narrow path as compared with the BC and SSC cases. The percentage error in the computed results was 6–8% and 3–5.5% for the SSC and LSC, respectively, indicating that the k–ω SST predicted successfully the flowfield characteristics. The results of the present study are also highly applicable to a wide range of applications including ground vehicles, suspension bridges, and buildings where unconfined flow conditions exists.

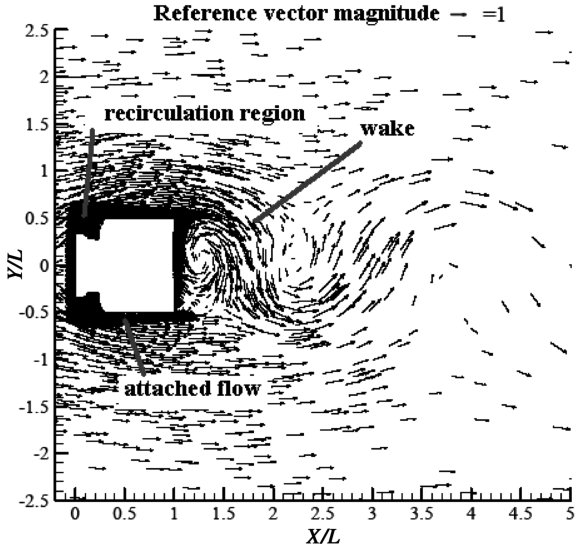

a) Computed velocity field

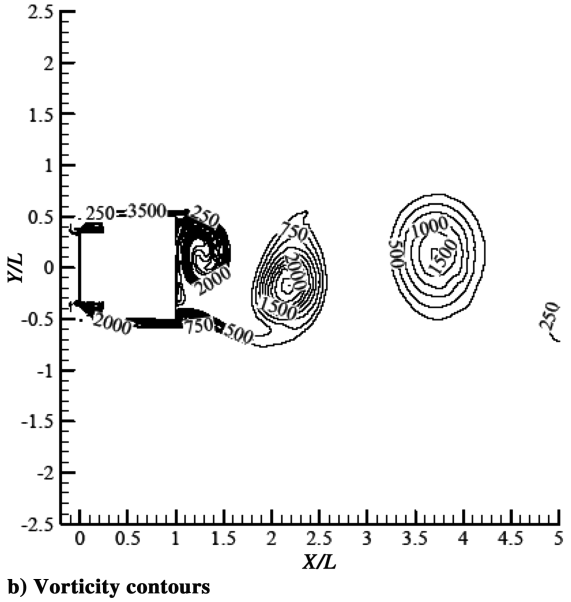

b) Vorticity contours

Fig. 3 Numerical flow visualization results for LSC case.

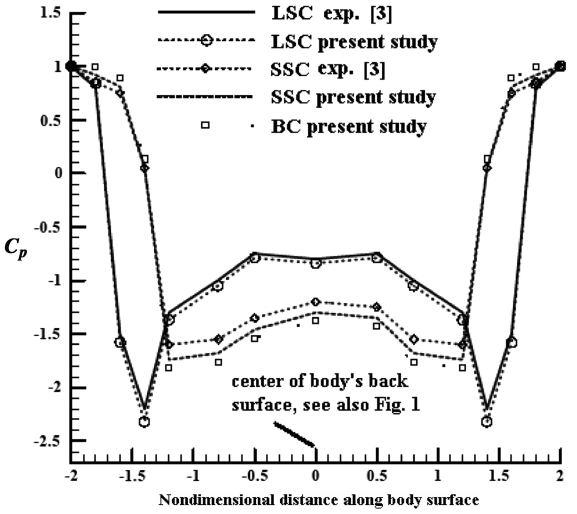

Fig. 4 Surface pressure coefficient distribution.

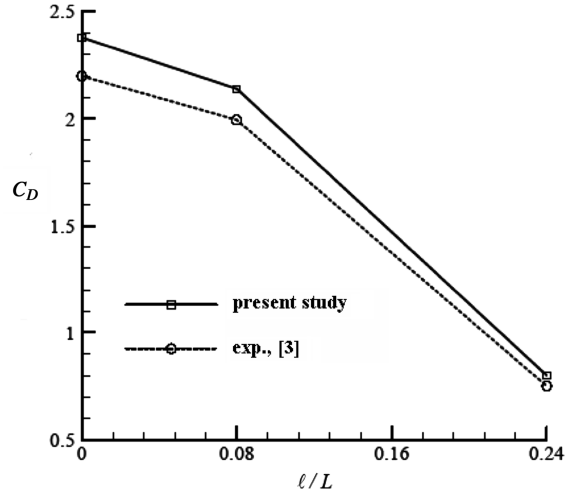

Fig. 5 Dependence of drag coefficient on step length.

References

[1] Gad-el-Hak, M., and Bushnell, D. M., "Separation Control Review," *Journal of Fluids Engineering*, Vol. 113, No. 5, 1991, pp. 5–30.

[2] Gad-el-Hak, M., "Modern Developments in Flow Control," *Applied Mechanics Reviews*, Vol. 49, No. 7, 1996, pp. 365–379.

[3] Anang, C., and Umemura, A., "Side Flow Stabilization of a Stepped-Nose Obstacle (Experimental Documentation)," *Transactions of the Japan Society for Aeronautical and Space Sciences*, Vol. 46, No. 153, 2003, pp. 163–172.

[4] Fluent 6.1 User's Guide, Fluent, Lebanon, NH, Dec. 2003.

[5] Leonard, B. P., "Stable and Accurate Convective Modeling Procedure Based on Quadratic Upstream Interpolation," *Computer Methods in Applied Mechanics and Engineering*, Vol. 19, No. 1, 1979, pp. 59–98.

[6] Rehman, A., "Computational Studies on the Control Effectiveness of Synthetic Jets for Aerodynamics Applications," Ph.D Dissertation, Univ. of Manchester, Manchester, England, U.K., Dec. 2004.

[7] Noack, B. R., Krig, M., and Eckelmann, H., "Three-Dimensional Stability Analysis of the Periodic Flow Around a Circular Cylinder," *Physics of Fluids A*, Vol. 5, No. 6, 1993, pp. 1279–128.

[8] Barkley, D., and Henderson, R. D., "Three Dimensional Floquet Stability Analysis of the Wake of a Circular Cylinder," *Journal of Fluid Mechanics*, Vol. 322, Sept. 1996, pp. 215–241.

[9] Mittal, R., and Balachandar, S., "Effect of Three-Dimensionality on the Lift and Drag of Nominally Two-Dimensional Cylinders," *Physics of Fluids*, Vol. 7, No. 8, 1995, pp. 1841–1865.